Remaining Useful Life Prediction of Battery Using a Novel Indicator and Framework With Fractional Grey Model and Unscented Particle Filter

Lin Chen, Jing Chen, Huimin Wang, Yijue Wang, Jingjing An, Rong Yang, and Haihong Pan

***Abstract*—The lithium-ion battery plays a crucial role in the power supply of the electric vehicles (EVs). Battery remaining useful life (RUL) is critically vital to ensure the vehicles' safety and reliability. Due to the complicated aging mechanism, predicting RUL for the battery management systems (BMSs) is challenging. In this article, a novel degradation indicator was constructed using the information extracted from the discharge voltage. The indicator reflected the complete and effective energy information from the voltage signals to reveal battery degradation characteristics. Additionally, an innovative fractional grey model (FRGM) unscented particle filter (UPF) framework was developed for RUL prediction in this article. To improve the accuracy and traceability of prediction, the framework adopted a novel FRGM to update the state transition equation in UPF. Meanwhile, the UPF was employed to extrapolate trends of the indicator and achieve the RUL prediction. The performances of FRGM-UPF with the degradation indicator were synthetically verified by the data from various types of batteries under different aging tests. The experimental results indicated that the proposed method could achieve precise prediction results and had a wide range of practicability and universality. The developed technologies could be incorporated with the other control algorithms for application in BMS of EVs.**

***Index Terms*—Discharge voltage, wavelet packet energy entropy (WPEE), fractional grey model (FGM), unscented particle filter (UPF), remaining useful life (RUL).**

NOMENCLATURE

RUL	Remaining useful life.
EV	Electric vehicle.
BMS	Battery management system.
PHM	Prognostics and health management.
GM	Grey model.
FRGM	Fractional grey model.
WPEE	Wavelet packet energy entropy.
PF	Particle filter.
UPF	Unscented particle filter.
UKF	Unscented Kalman filter.
CC	Constant current.
CV	Constant voltage.
NEDC	New European driving cycle.
UDDS	Urban dynamometer driving schedule.
JP1015	Japanese 1015 mode driving schedule.
AMPSO	Adaptive mutation particle swarm optimizer.
PSP	Prediction start point.
AE	Absolute error.
EM-PF	Exponential model-particle Filter.

Manuscript received June 3, 2019; revised September 8, 2019; accepted October 27, 2019. Date of publication November 10, 2019; date of current version February 20, 2020. This work was supported by the National Natural Science Foundation of China under Grant 51667006. Recommended for publication by Associate Editor W. Cao. *(Corresponding author: Haihong Pan.)*

L. Chen is with the Department of Mechatronics Engineering, College of Mechanical Engineering, Guangxi University, Nanning 530000, China, and also with the Guangxi Key Laboratory of Electrochemical Energy Materials, Collaborative Innovation Center of Renewable Energy Materials, Guangxi University, Nanning 530000, China (e-mail: gxdxcl@163.com).

J. Chen, H. Wang, J. An, R. Yang, and H. Pan are with the Department of Mechatronics Engineering, College of Mechanical Engineering, Guangxi University, Nanning 530000, China (e-mail: 492451425@qq.com; wanghmhit@foxmail.com; andwyane@163.com; yangrong0907@163.com; hustphh@163.com).

Y. Wang is with the Department of Computer Science and Engineering, University of Connecticut, Storrs, CT 06269 USA (e-mail: yijue.wang@uconn.edu).

This article has supplementary downloadable material available at http://ieeexplore.ieee.org.

Color versions of one or more of the figures in this article are available online at http://ieeexplore.ieee.org.

Digital Object Identifier 10.1109/TPEL.2019.2952620

I. INTRODUCTION

EQUIPPED with high energy density, high galvanic potential and long lifetime, lithium-ion batteries have been applied to many industrial areas as power sources [1]–[3]. Typically, lithium-ion batteries have become key components of electric vehicles (EVs) and plug-in hybrid EVs. Nevertheless, they endure continuous performance degradation throughout their whole service life due to the inevitable side reactions. Consequently, the prognostics and health management (PHM) is essential to the battery system, which can reduce battery operating risk and ensure battery reliability under current life-cycle conditions [4]. Remaining useful life (RUL) prediction is an important part for PHM, which refers to the available service time left before the capacity fade reaches an unacceptable level [5]. Reliable RUL prediction is of great significance for scheduling repairs and maintenance in advance and providing an alarm before faults reach critical levels [6], [7].

At present, the commonly used RUL prediction methods can be roughly classified into model-based methods and data-driven methods [8]. The model-based methods usually start with the construction of the battery degradation models, then filtering techniques are employed to track the degradation trend, for they can not only track the system states, but also, deal with the nonlinear non-Gaussian issue. For example, Goebel *et al.* [9] built an impedance-based exponential model for battery and applied the particle filter (PF) to track and update the model

parameters. Then, the RUL is derived by extrapolating out the capacity calculated by model parameters into the future until it hits a predetermined end-of-life threshold. Nevertheless, the standard PF may endure decrease in prediction accuracy due to the ever-presence of particle weights degradation. To solve this issue, Miao *et al*. [10] proposed an unscented particle filter (UPF) algorithm, which adopted the unscented Kalman filter (UKF) results as the proposal distribution of PF. This method was proved to be effective for tracking the parameters of exponential capacity model and improving the accuracy of the RUL prediction. Based on the same battery model, Zhang *et al*. [11] predicted the battery RUL through a promoted UPF, which effectively overcame the loss of particle diversity in UPF via the linear optimizing combination resampling technique. Lacking the description of battery degradation mechanisms, these employed exponential models can hardly reflect the characteristics of parameters evolution accurately. From the aspect of improving battery degradation model, Lyu *et al*. [12] proposed an electrochemical model to simulate the battery degradation process, then an improved PF framework was utilized to estimate the model parameters that are the characterization of battery internal degradation. Guha *et al*. [13] presented a fractional-order equivalent circuit model to estimate the electrochemical impedance spectrum (EIS) of the battery. The estimated EIS was used to establish a regression model to represent the degradation trend and the regression model was combined with the PF framework to predict RUL.

Unlike the model-based algorithms, the data-driven methods take advantage of advanced machine learning algorithms to achieve RUL prediction with available historic data, and they are not dependent on models featuring degradation-dependent parameters. Recently, the support vector machine (SVM) [14], [15], relevance vector machine [16], and neural networks [17], [18] have become the most common data-driven methods for their good adaptability. Patti *et al*. [14] presented a multistage SVM approach which employed a novel classification model to provide a gross estimation for RUL, and then, the regression model of SVM was utilized to generate an accurate RUL estimate. Wei *et al*. [15] built an SVR-based battery capacity degradation model to simulate the battery aging mechanism and estimate the state-of-health and RUL. To reduce the computational complexity of the kernel function and improve the online learning capability, Liu *et al*. [16] proposed an incremental optimized RVM method, which implemented a flexible on-line training strategy for RUL prediction. Zhang *et al*. [17] proposed a long short-term memory (LSTM) recurrent neural network to establish a capacity-oriented RUL predictor and then adopted the Monte Carlo simulation to generate the probability distribution of RUL prediction results. Similarly, Li *et al*. [18] presented a novel hybrid Elman-LSTM method for battery RUL prediction. They employed the recurrent LSTM and Elman neural networks to predict the capacity sub-layers decomposed by the empirical model decomposition. These data-driven methods usually require a large quantity of recorded data to predict the battery degradation trend.

Most of the presented methods used capacity directly as the indicator to quantify the battery degradation and to predict the RUL. However, it is difficult to monitor and measure the capacity data of batteries accurately under practical dynamic conditions. In this regard, some directly measured parameters of the battery have been utilized for RUL prediction [19]. For instance, Lin *et al*. [20] analyzed the battery's data including the constant current charge time, the instantaneous voltage drop and the open circuit voltage, then they used these data as the input of probabilities neural network to achieve capacity estimation. Although these parameters could effectively quantify the battery degradation, the amount of required data is too large. To simplify the types and amount of data, some scholars extracted or transformed these measured data as a new type of degradation characterization. Zhou *et al*. [7] and Liu *et al*. [21] quantified the capacity degradation for online RUL prediction through the voltage falloff of equal time interval. Hu *et al*. [6], [22] pointed out how to use the sample entropy of short voltage sequence as an effective signature of capacity loss. The existing methods usually solely analyze part of the measurable data, which improves the operability but may result in an incomplete description of the degradation information. Nevertheless, these novel methods provided by the prior studies have inspired new ideas and made great contributions to the RUL prediction.

To enhance the accuracy and robustness of the RUL prediction, more issues need to be solved. For instance, most measured parameters are not able to characterize battery degradation directly, especially when the historical data are small in the initial stages of prediction. Lithium-ion battery degradation exhibits time-varying and nonlinear characteristics. Traditional degradation models like exponential model are hard to completely describe the degradation performances of battery under practical circumstances. To find solutions for these issues, this article proposed a novel RUL prediction method from two corresponding perspectives. First, we extracted the wavelet packet energy entropy (WPEE) of the discharge voltage data as a new indicator for quantifying battery degradation. The indicator reflected the complete and effective information entropy from the voltage signals, which revealed battery degradation characteristics from the view of information changes in energy. Second, a fractional grey model (FRGM) was developed to simulate the evolution trend of WPEE during the battery full-life cycle, so as to reflect the complex degradation process of capacity. Without the exploration in internal degradation mechanism, the FRGM could achieve the superiority of both simplicity and high precision at dynamic conditions. Based on these main contributions, the UPF was introduced to establish an FRGM-UPF framework by reconstructing its state transition equation using the FRGM, and then the WPEE was extrapolated by the framework to generate RUL prediction. Moreover, experimental data sets from various types of batteries under three aging test conditions were applied to evaluate the performance of FRGM-UPF framework and to verify its effectiveness and universality.

The remainder of this article is structured as follows. The battery experiments are introduced in Section II. Section III describes the novel method for RUL prediction in detail. The RUL prediction with the proposed method is performed in Section IV. Finally, Section V concludes this article.

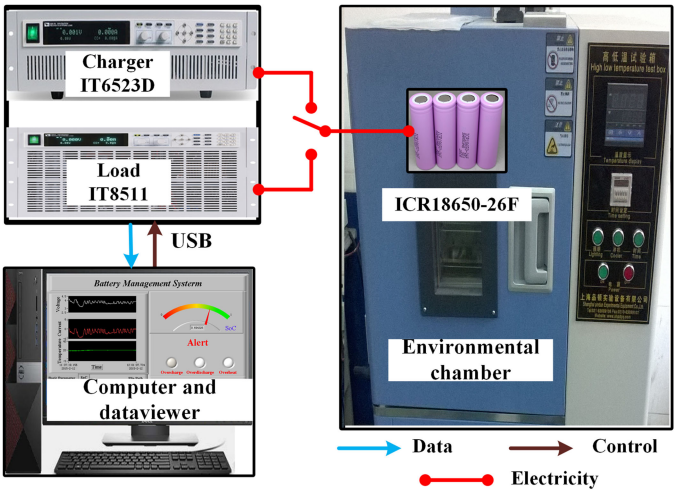

Fig. 1. Physical experimental platform.

TABLE I
MAJOR EQUIPMENT PARAMETERS

Device name	IT6523D	IT8511
Maximum voltage (V)	160 V ± 0.2% full scale	120 V ± 0.05% full scale
Maximum current (A)	120 A ± 0.2% full scale	30 A ± 0.1% full scale
Voltage accuracy (V)	±(0.05%+5mV)	±(0.05%+0.02% full scale)
Current accuracy (A)	±(0.1%+10mA)	±(0.05%+0.05% full scale)

TABLE II
MAIN SPECIFICATIONS OF THE LITHIUM-ION BATTERIES

No.	Nominal capacity (Ah)	Charge cut-off voltage (V)	Discharge cut-off voltage (V)	Capacity failure threshold (Ah)
B06	2	4.2	2.50	1.40
B07	2	4.2	2.20	1. 42
P01	3.3	4.2	2.50	2.76
S17/S42/S43	2.6	4.2	2.75	2.08

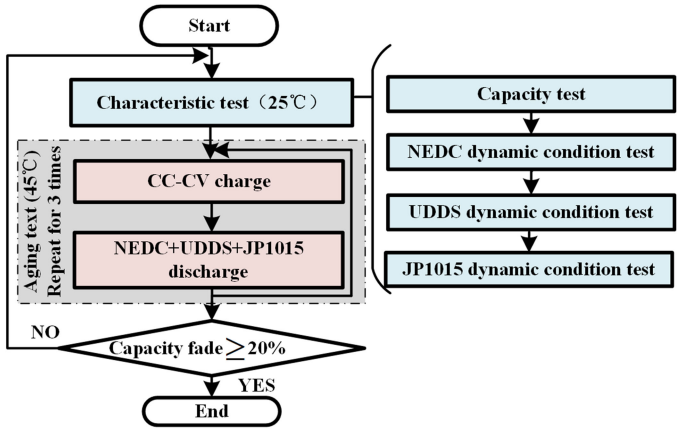

Fig. 2 Battery test schedule for S42 and S43.

II. EXPERIMENTAL DESIGN

A. Experimental Platform

The experimental platform consists of an environmental chamber (GDW-100L) for environment control, batteries, a charger (ITECH IT6523D), an electronic load (ITECH IT8511), and a computer for user-machine interface and data storage (see Fig. 1). The environment chamber can provide an accuracy of ±0.5 °C over a full −40 °C to 150 °C temperature range. The major parameters of the the charger and load are given in Table I.

The datasets of batteries include terminal voltage (V), load current (A), discharge capacity (Ah), and temperature (°C), which are collected and recorded during charge and discharge. The data acquisition frequency is 1 Hz, and the recorded data are transmitted to the control computer via a USB cable.

B. Battery Tests

Two types of data sets were studied in this article. The specific parameters of batteries were given in Table II.

1) One dataset was obtained from the data repository of the NASA Ames Prognostics Center of Excellence, the tested batteries were lithium-nickel-cobalt-aluminum 18650-size batteries [23]. The samples B06 and B07 were tested at room temperature. Charge was carried out in a constant current (CC) mode at 1.5 A until the voltage reached 4.2 V. The battery continued in a constant voltage (CV) mode until the charge current dropped to 20 mA. Discharge was undertaken in a CC mode at 2 A until the battery voltage fell to 2.5 and 2.2 V, respectively. The battery was charged and discharged repeatedly until it reached the end-of-life with a 30% fade of rated capacity.
2) Another dataset was from the experimental platform, as shown in Fig. 1. Two types of 18650 Li-ion cells were selected for dynamic current tests. The batteries included lithium cobalt oxide batteries (S17, S42, and S43) and lithium-nickel-manganese-cobalt battery (P01).

These four batteries were divided into two groups based on different aging tests and were tested separately. In each group of aging tests, batteries were placed in a chamber and they were tested independently. For the battery S17 and P01, the characteristic cycle was composed of a capacity test and a new European driving cycle (NEDC) test at 25 °C. Their aging tests were repeated using a CC–CV charge and a 5.2 A discharge. These tests were executed until their capacities declined to the capacity failure threshold. Another aging test (see Fig. 2) was designed for S42 and S43, and the test cycle primarily covered the characteristic test and the aging cycle test. The characteristic test was carried out at 25 °C, which included the capacity test, NEDC test, urban dynamometer driving schedule (UDDS) test and Japanese 1015 mode driving schedule (JP1015) test. The aging cycle test was performed at 45 °C, and it was repeated three times for each cycle. The mode of charge and discharge was composed of a constant current, a constant voltage

TABLE III
COMPARISONS OF DIFFERENT BATTERY TESTS

Battery No.	Characteristic test		Aging test	
	Loading profile	Ambient temperature	Loading profile	Ambient temperature
B06/B07	\	\	CC-CV charge/ 2A discharge	24°C
P01/S17	Capacity test/ NEDC	25°C	CC-CV charge/ 5.2A discharge	45°C
S42/S43	Capacity test/ NEDC/UDDS/ JP1015	25°C	CC-CV charge/ mixed dynamic current discharge	45°C

(CC–CV) charge, and a mixed dynamic current discharge (including NEDC, UDDS, and JP1015). The comparisons of three different battery tests are given in Table III.

III. METHODOLOGY

A. Wavelet Packet Energy Entropy

Commonly, for a new lithium-ion battery, the operating time (discharge time period) is maximal after a full charge at the very beginning. The operating time after subsequent full charge becomes shorter and shorter due to the charge and discharge process [7]. This is because the maximum charge capacity fades with the cyclic charge and discharge. During the discharge period, it is normal that as the battery fades, the measurable voltage response alters accordingly under the same excitation [6].

Owing to the complexity and fluctuation of the alteration, the WPEE method was proposed to capture the alterations of the discharge voltage response to battery fades. The theory of WPEE is the combination of wavelet packet decomposition [24], [25] and information entropy theory [26]. Wavelet packet decomposition is a signal decomposition method, which was able to eliminate the interference of uncorrelated noise by simultaneously decomposing and reconstructing the high and low-frequency parts of the signal. Wavelet packet decomposition can reflect the complete and effective energy information. Information entropy is the quantity that describes the state of energy degradation of a substance. In this article, information entropy was used to measure the uncertainty and energy changes of the signals. The WPEE revealed the degradation trends of the battery through extracting information from discharge voltage. The Box-Cox nonlinear transformation was adopted to obtain the failure threshold value of WPEE for RUL prediction.

1) Specific Process of WPEE Extraction: According to the Shannon information entropy theory [26], the WPEE is defined as follows:

$$H_{jh} = -\sum_{i=1}^{N} \varepsilon_{jh}(i)\, lg \varepsilon_{jh}(i) \tag{1}$$

where H_{jh} is the *j*th layer of the signal and the *h*th WPEE; the value of *h* ranges in $[0, 2^j - 1]$; *N* is the original signal length; $\varepsilon_{jh}(i)$ represents the normalized wavelet coefficients on the *h*th band of the *j*-layer [27] and is defined as

$$\varepsilon_{jh}(i) = \frac{E(i)}{\sum_{i=1}^{2^j-1} E(i)} \tag{2}$$

where E_i is the energy spectrum of the signal at various scales. It denotes a division of the signal energy in the scale domain.

The discharge voltage signal is decomposed by the *j*-layer wavelet decomposition to get the *h*th WPEE of the *j*th layer [24], [25]

$$e_{jh} = -\sum_{i=1}^{N} \varepsilon_{jh}(i)\, lg \varepsilon_{jh}(i). \tag{3}$$

The WPEE of the *k*th cycle is expressed as $e_{\mathrm{vol}}(k)$

$$e_{\mathrm{vol}}(k) = \sum_{h=0}^{2^j-1} e_{jh}. \tag{4}$$

To enable that the acquired WPEE values be compared or analyzed at the same level, a data normalization processing is performed on the extracted WPEE of each discharge cycle

$$E_{\mathrm{vol}}(k) = \frac{e_{\mathrm{vol}}(k) - \min\limits_{1\le i\le l}\{e_{\mathrm{vol}}(i)\}}{\max\limits_{1\le i\le l}\{e_{\mathrm{vol}}(i)\} - \min\limits_{1\le i\le l}\{e_{\mathrm{vol}}(i)\}} \tag{5}$$

where $k = 1, 2, 3 \ldots l$; the WPEE series can be expressed as: $E_{\mathrm{vol}} = \{E_{\mathrm{vol}}(1), E_{\mathrm{vol}}(1), \ldots, E_{\mathrm{vol}}(l)\}$.

2) Exploration of the Failure Threshold of WPEE: According to the original Box-Cox transformation formula [28], a linear model is constructed as (6). The battery capacity C is conversion variable and the normalized WPEE E_{vol} is the independent variable

$$C(\lambda) = \beta_0 + \beta_1 E_{\mathrm{vol}} + \eta = \mathbf{X}\boldsymbol{\beta} + \eta$$
$$\eta \sim N(0, \sigma^2), \quad \mathbf{X} = [1, E_{\mathrm{vol}}], \quad \boldsymbol{\beta} = [\beta_0, \beta_1]^T \tag{6}$$

where $C(\lambda)$ represents the capacity after transformation; $\boldsymbol{\beta}$ is the regression sample parameter; η is the random error following the principle of normal distribution; and σ^2 is the root mean square error. Where λ can be obtained by the maximum likelihood estimation; $\boldsymbol{\beta}$ and σ^2 can be obtained by the least squares method [29].

With the parameters of λ, $\boldsymbol{\beta}$, and σ^2, the failure threshold of capacity is obtained after transformation $C_T(\lambda)$

$$C_T(\lambda) = \begin{cases} \frac{C_T^{\lambda}-1}{\lambda}, & \lambda \neq 0 \\ \log C_T, & \lambda = 0. \end{cases} \tag{7}$$

Ultimately, the failure threshold of WPEE $E_{\mathrm{vol}}(t)$ can be determined and calculated by

$$C_T(\lambda) = \beta_0 + \beta_1 \mathbf{E_{vol}} + \varepsilon = \mathbf{X}_T\boldsymbol{\beta} + \eta \tag{8}$$

where $\mathbf{X}_T = [1, E_{\mathrm{vol}}(t)]$.

B. Establishment of the FRGM

To predict the RUL rapidly and accurately over the lifetime of a battery, in this article, the grey system theory is applied

since it requires less data and it is independent of the accuracy of the model's parameters [30]. The FRGM is built, based on the GM(1, 1), which is one of the most efficient grey models [31]. To better track battery degradation, the adaptive mutation particle swarm optimizer (AMPSO) [32] is adopted to update the model parameter at different prediction start points (PSPs) of the FRGM. The modeling procedures of FRGM are described as follows.

$E_{\text{vol}} = [E_{\text{vol}}^{(0)}(1), E_{\text{vol}}^{(0)}(2), \ldots, E_{\text{vol}}^{(0)}(k)]$ is the historical array sequence, and the r-order cumulative generation sequence of historical array sequence is expressed as

$$E_{\text{vol}} = \left[E_{\text{vol}}^{(r)}(1), E_{\text{vol}}^{(r)}(2), \ldots, E_{\text{vol}}^{(r)}(k)\right] \tag{9}$$

where

$$E_{\text{vol}}^{(r)}(h) = \sum_{i=1}^{k} \frac{\Gamma(r+h-i)}{\Gamma(h-i+1)\Gamma(r)} E_{\text{vol}}^{(0)}(i), \quad h = 1, 2, 3, \ldots, k \tag{10}$$

where $\Gamma(\cdot)$ is the gamma function and the second integral of Euler. r is the fractional order. The whitening differential equation is given by

$$\frac{dE_{\text{vol}}^{(r)}(k)}{dt} + aE_{\text{vol}}^{(r)}(k) = b \tag{11}$$

where the AMPSO is used to optimize r; a is the development coefficient, representing the development trend of historical sequence; and b is a constant coefficient indicating the influence of the external impact on the development of an event. To obtain the essential parameter, the sequence of parameters $\hat{a} = [a, b]^T$ is calculated as follows:

$$\hat{a} = (\mathbf{B}^T \times \mathbf{B})^1 \times \mathbf{B}^T \times \mathbf{Y}_S \tag{12}$$

where

$$\mathbf{B} = \begin{bmatrix} -0.5 \times (E_{\text{vol}}^{(r)}(2) + E_{\text{vol}}^{(r)}(1)) & 1 \\ -0.5 \times (E_{\text{vol}}^{(r)}(3) + E_{\text{vol}}^{(r)}(2)) & 1 \\ \vdots & \vdots \\ -0.5 \times (E_{\text{vol}}^{(r)}(k) + E_{\text{vol}}^{(r)}(k-1)) & 1 \end{bmatrix} \tag{13}$$

and

$$\mathbf{Y}_S = \left[E_{\text{vol}}^{(0)}(2)\ E_{\text{vol}}^{(0)}(3) \cdots E_{\text{vol}}^{(0)}(k)\right]^T. \tag{14}$$

According to (9), the forecasting value of the whitening differential equation is acquired as follows:

$$\hat{E}_{\text{vol}}^{(r)}(k+1) = \left(E_{\text{vol}}^{(0)}(1) - \frac{b}{a}\right) \times e^{-ak} + \frac{b}{a}. \tag{15}$$

To calculate the forecasting values of $\hat{E}_{\text{vol}}^{(0)}(k+1)$, the inverse accumulated generating operation is used

$$\hat{E}_{\text{vol}}^{(0)}(k+1) = \left[\hat{E}_{\text{vol}}^{(r)}(k+1)\right]^{(-r)} = \sum_{i=0}^{k} (-1)^i \frac{\Gamma(r+1)}{\Gamma(i+1)\Gamma(r-i+1)} \hat{E}_{\text{vol}}^{(r)}(k+1-i). \tag{16}$$

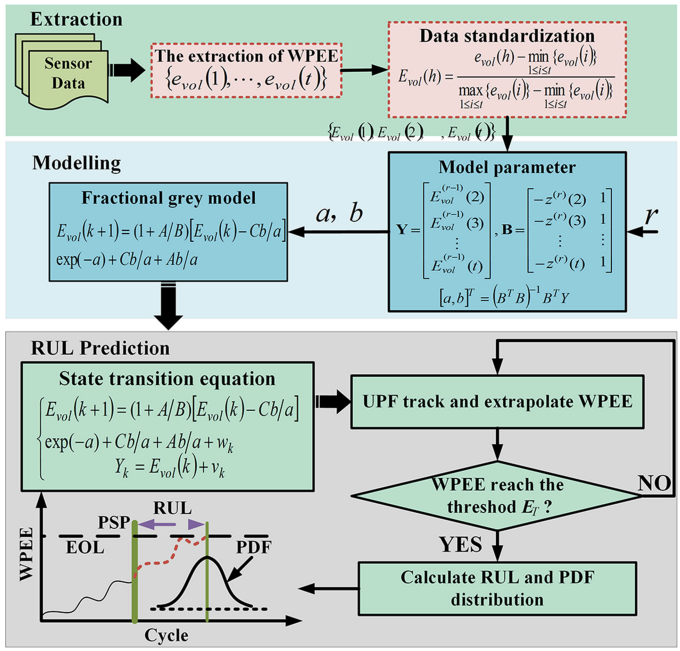

Fig. 3. FRGM-UPF framework for RUL prediction.

Therefore, for this study the battery degradation model is expressed as

$$E_{\text{vol}}(k+1) = (1 + A/B)(E_{\text{vol}}(k) - Cb/a)\exp(-a) + Cb/a + Ab/a \tag{17}$$

where A, B, and C are model coefficients

$$\begin{cases} A = (-1)^k \frac{\Gamma(r+1)}{\Gamma(i+1)\Gamma(r-i+1)} \\ B = \sum_{i=0}^{k-1} (-1)^i \frac{\Gamma(r+1)}{\Gamma(i+1)\Gamma(r-i+1)} \exp(-a(k-i)) \\ C = \sum_{i=0}^{k-1} (-1)^i \frac{\Gamma(r+1)}{\Gamma(i+1)\Gamma(r-i+1)}. \end{cases} \tag{18}$$

C. FRGM-UPF With WPEE for RUL Prediction

PF is a general algorithm based on the recursive Bayesian estimation, focusing on a general situation of nonlinear state-space model and non-Gaussian noise assumption. UPF is established on the theories of PF and UKF algorithms. To obtain the posterior probability of the latest observation, the UKF algorithm was first applied to generate a proposal distribution. The PF algorithm was used to get the prediction results. The method proposed in this article adopted the FRGM to construct the state transition equation of UPF. The framework of proposed FRGM-UPF is shown in Fig. 3.

The specific implementation processes for battery RUL prediction are as follows.

Step 1: Extracting the WPEE from battery discharge voltage $E_{\text{vol}} = [E_{\text{vol}}(1), E_{\text{vol}}(2), \ldots, E_{\text{vol}}(k)]$.

Step 2: With the historical WPEE, the development coefficient a, constant coefficient b and optimization order r can be calculated. The state transition equation of UPF is developed based on the (17) exhibiting

as follows:

$$\begin{cases} E_{\text{vol}}(k+1) = (1+A/B)(E_{\text{vol}}(k) - Cb/a)\exp(-a) \\ \qquad\qquad + Cb/a + Ab/a + w_k \\ Y_k = E_{\text{vol}}(k) + v_k \end{cases} \tag{19}$$

where $E_{\text{vol}}(k+1)$ denotes the WPEE estimated at the cycle $k+1$ and the y_k denotes the WPEE measured at cycle k; v_k is the process noise; and w_k indicates the measurement noise.

Step 3: FRGM-UPF for RUL prediction

1) Initialize PF: $K = 0$ and set the initial weights to $w_0^i = 1/N, i = 1, 2, \ldots, N$.
2) Use the UKF algorithm to get the proposal distribution. Take the UKF steps and get $E_{\text{vol}}^i(k+1)$ and $\hat{p}_{k+1}^i$.
3) Take the PF steps to get the final particles and weights. The state and its covariance can be calculated by:

$$\hat{E}_{\text{vol}}(k+1) = \sum_{i=1}^{N} \tilde{w}_{k+1}^i E_{\text{vol}}^i(k+1) \tag{20}$$

$$P_{k+1} = \sum_{i=1}^{N} \tilde{w}_{k+1}^i \left(E_{\text{vol}}^i(k+1) - \hat{E}_{\text{vol}}(k+1)\right) \times \left(E_{\text{vol}}^i(k+1) - \hat{E}_{\text{vol}}(k+1)\right)^T. \tag{21}$$

4) Estimate the posterior PDF of RUL at the cycle $k+1$

$$p(\text{RUL}|\, y_{1:k+1}) \approx \sum_{i=1}^{N} \omega_{k+1}^i \delta\left(\text{RUL}_{k+1} - \text{RUL}_{k+1}^i\right). \tag{22}$$

The expectation of RUL is approximated by

$$\hat{\text{RUL}}_{k+1} = \sum_{i=1}^{N} \text{RUL}_{k+1}^i \omega_{k+1}^i. \tag{23}$$

The RUL is the RUL before the WPEE hits the pre-defined performance threshold.

IV. Results and Discussion

In the current research, the novel battery indicator (WPEE) extracted from discharge voltage was employed to characterize the battery degradation. The FRGM-UPF framework was used to predict the battery RUL. In this section, the authors analyzed the effectiveness of WPEE and verified the accuracy of FRGM. Additionally, the RUL prediction method (FRGM-UPF) was confirmed with different batteries and various PSPs, such as 1/3, 1/2, and 2/3 of the full life cycle.

A. Analyses of FRGM Applied to WPEE Prediction

The degradation trends of capacity and WPEE for different batteries are displayed in Fig. 4. The WPEE shows a roughly linear upward trend, which is negatively associated with the degradation curve of battery capacity. The degradation

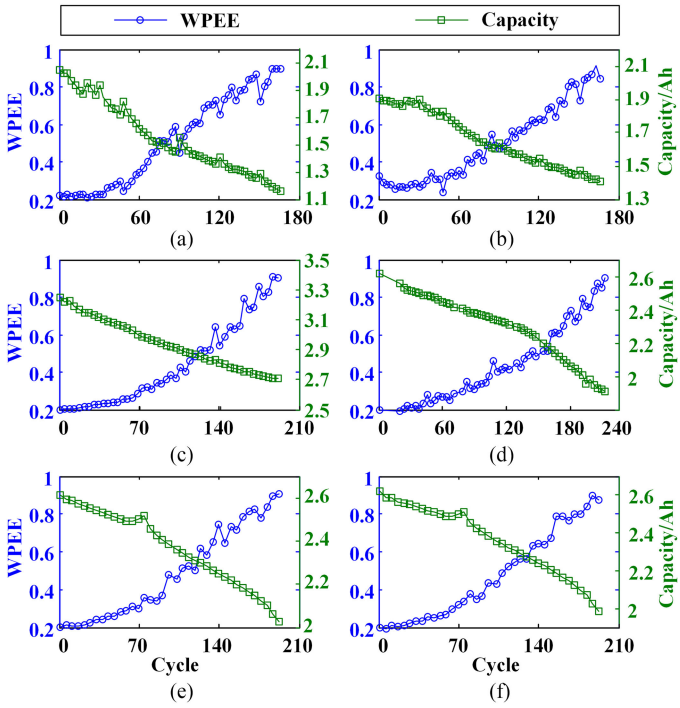

Fig. 4. Battery capacity and extracted WPEE.

trajectories of batteries show strongly nonlinear due to the discontinuity of aging tests, and the degradation level of batteries have some partial rebounds. The intuitive manifestation of this phenomenon is the capacity regeneration, which can be directly observed in Fig. 4(a) and (b) and (e) and (f). In this case, the discharge voltage waveform of each cycle will change with the fluctuation of the battery degradation level. Consequently, the frequency band energy contained in the voltage waveform will fluctuate to varying degrees in both numerical value and distribution pattern, which is reflected in the WPEE and makes it show an upward trend with some fluctuations. For example, the capacities of B06 and B07 fluctuates are more frequently than the other batteries, therefore, the corresponding WPEE fluctuates more frequently than the other batteries do, as shown in Fig. 4(a) and (b). Additionally, P01 and S17 are tested at the same profiles and experimental conditions, but their capacity and WPEE trajectories are distinctly diverse since they are different on components and specification parameters. For batteries S42 and S43, it shows the similar capacity and WPEE trends under the same experimental conditions.

WPEE are linearly related to the capacity under different aging tests, and the WPEE increases with the decrease of capacities for the life cycles. Their expressions of linear fitting are shown in Fig. 5. For different aging tests or different type of batteries, the absolute values of the slope of linear fitting are obviously different. For the same type of batteries (such as S42 and S43), the batteries were tested under the same conditions. The absolute values of their slopes are similar, and the difference is only 0.046544 [see Fig. 5(c)]. However, the same type of batteries (such as S17 and S42) under different aging tests, the slope values of the two lines are fairly different, as shown in Fig. 5(b) and (c). In Fig. 5(b), it can be seen that the intercept and the

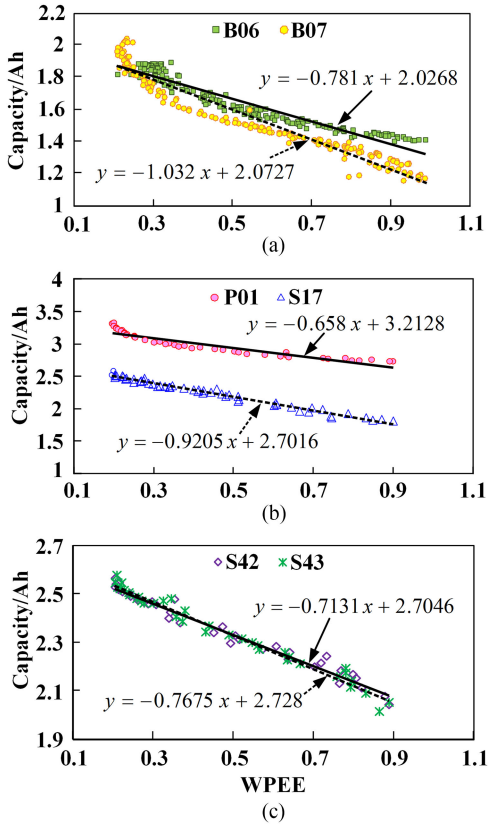

Fig. 5. Linear correlation between WPEE and capacity.

TABLE IV
CORRELATION ANALYSIS

No.	B06	B07	P01	S17	S42	S43
r	-0.963	-0.956	-0.930	-0.989	-0.987	-0.989
r_s	-0.986	-0.971	-0.996	0.950	-0.986	-0.992

slopes of two fitting lines are obviously disparate for different types of batteries (P01 and S17) under the same test conditions.

To validate the correlation between WPEE and capacity, the quantitative assessments are performed by Pearson (r) and Spearman (r_s) correlation coefficients is given in Table IV. Pearson correlation coefficient is used as a quantitative validation of the linear relationship. The value of r is between $[-1, 1]$, and a greater absolute value of r indicates there is a better linear relationship between WPEE and capacity. Additionally, Spearman correlation coefficient is a nonparametric way to assess the strict monotonic relationship between WPEE and capacity. Similarly, the value of r_s is between $[-1, 1]$, and greater absolute value of r_s means stricter monotonic relationship. Since the r and r_s of all the batteries under different aging tests are above 0.93, it indicates that that WPEE and capacity are strongly correlated. As a result, the WPEE values of discharge voltage can characterize the real-time degradation process of batteries effectively, similar as the capacity can quantify the actual battery degradation.

The accuracy of this model needs to be verified before using FRGM as the UPF state space equation to perform the battery RUL prediction. The historical WPEE values (different PSPs) are used for initialization of FRGM, and the FRGM method is

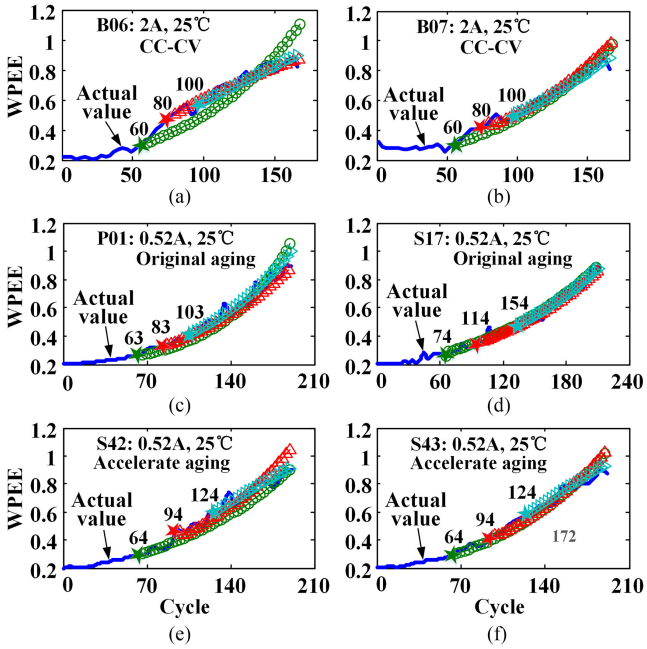

Fig. 6. WPEE prediction results based on FRGM for six batteries at different PSPs.

TABLE V
FRGM PERFORMANCE EVALUATION RESULTS

Index	PSP	B06	B07	P01	S17	S42	S43
RMSE	1/3	0.106	0.053	0.060	0.032	0.061	0.048
	1/2	0.036	0.051	0.033	0.028	0.070	0.055
	2/3	0.041	0.033	0.049	0.028	0.034	0.036
R^2	1/3	0.886	0.881	0.898	0.967	0.889	0.929
	1/2	0.904	0.891	0.962	0.965	0.889	0.942
	2/3	0.951	0.908	0.889	0.950	0.897	0.952

applied to predict the WPEE shown in Fig. 6. The prediction results basically coincide with the actual values, indicating the FRGM can precisely predict the WPEE. However, some prediction results still have large errors. Take B06 and S42 for example, when the starting point of the model at 1/3 full life cycle, the predicted values are significantly different from the actual values. The FRGM is difficult to accurately predict the WPEE. Nevertheless, when using more data, the prediction results became more accurate. The root of the mean square (RMSE) and goodness of fit (R_2) are applied to further evaluate the performance of the prediction of FRGM (see Table V). The overall R^2 values are between 0.881 and 0.967, indicating adequate statistical fit. The RMSE values are between 0.028 and 0.106, exhibiting high precision of the prediction results. Both criteria indicate that the FRGM has a high modeling accuracy. Evidently, these analyses illustrate the FRGM perform superiorly in prediction. Because the WPEE is used to represent the actual battery degradation, the battery degradation trend can be effectively predicted by FRGM.

B. RUL Prediction With FRGM-UPF

In this section, the RUL prediction is carried out to validate the effectiveness of the FRGM-UPF framework with WPEE.

TABLE VI
RUL PREDICTION RESULTS OF B06 COMPARED WITH FRGM-PF WITH WPEE AND [33]

Algorithm	Time complexity	PSP	RUL	$\hat{\text{RUL}}$	AE
FRGM-UPF with WPEE	O (n^3)	60	48	54	6
		80	28	25	3
		100	8	7	1
FRGM-PF with WPEE	O (n^3)	60	48	56	8
		80	28	22	6
		100	8	10	2
EM-PF with capacity [29]	O (n^2)	60	48	57	9
		80	28	18	10
		100	8	5	3

The prediction results of B06 using FRGM-UPF with WPEE proposed in this article are compared with the other two methods, including the EM-PF [33] and the FRGM-PF algorithm (the combination of our FRGM and the PF from [33]). The results are displayed in Table VI. The absolute error (AE) is used as an evaluation criterion to assess the accuracy of the prediction results quantitatively. The AE was calculated by

$$\text{AE} = |\text{RUL} - \hat{\text{RUL}}| \tag{24}$$

where RUL is the actual RUL value and $\hat{\text{RUL}}$ is the predicted RUL value.

The RUL prediction results indicate that the proposed FRGM-UPF with WPEE has better RUL prediction accuracy than the other two methods, and the contrastive FRGM-PF show superiority over the EM-PF. Unlike the fluctuant errors of EM-PF with capacity, the prediction errors of FRGM-UPF with WPEE and FRGM-PF with WPEE are obviously decreased as the historical data increase, the AE of FRGM-UPF and FRGM-PF achieve, respectively, 1 and 2 cycles when the PSP is 100. The prediction results of FRGM-UPF are superior to the FRGM-PF at all PSPs. In terms of computational complexity, the maximum time complexity of FRGM-UPF is O (n^3) (n is the number of input data), while that of traditional EM-PF is O (n^2), which means that the FRGM-UPF algorithm needs an additional computational process for input data, and its running time is longer. But the synergy of FRGM-UPF and WPEE performs much better in accuracy and convergence than EM-PF, the extra computing time brought by the algorithm is acceptable.

To further verify the effectiveness and universality of proposed FRGM-UPF with WPEE, RUL prediction results of six batteries at different PSPs are shown in Fig. 7. The AE is used for the quantitative assessment of prediction accuracy (see Table VII).

For the prediction of B06 and B07 at CC aging tests Fig. 7(a) and (b), in general, the prediction trajectories are satisfactory except the result of B06 at the PSP of 60. This outlier trajectory has deviated significantly from the true value, and the AE is six cycles. The AEs of the most prediction results are no more than five cycles. Similar to [7] and [33], at the beginning of the prediction, the models are initialized by a few training data and the AE was relatively large. With the growth of the cycles, the prediction accuracy became significantly better. These results indicate that the prediction accuracy is highly dependent on the amount of data. However, the FRGM have the ability of mining

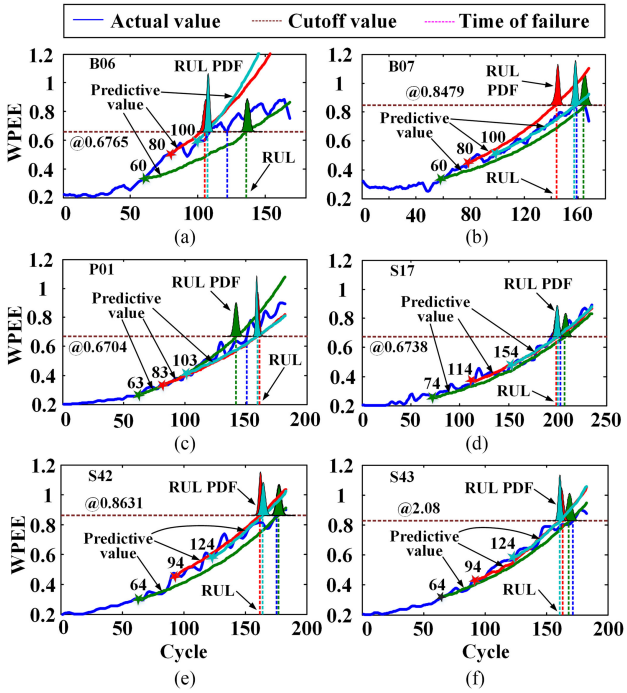

Fig. 7. RUL prediction results based on FRGM-UPF with WPEE for six batteries at different PSPs.

TABLE VII
RUL PREDICTION RESULTS BASED ON FRGM-UPF AT DIFFERENT PSPS

No.	PSP	RUL	$\hat{\text{RUL}}$	AE
B07	60	99	105	6
	80	79	74	5
	100	59	57	2
P01	63	88	82	6
	83	68	75	7
	103	48	52	4
S17	74	129	124	5
	114	89	85	4
	154	49	46	3
S42	64	112	120	8
	94	82	76	6
	124	52	48	4
S43	64	108	99	9
	94	78	72	6
	124	48	53	5

underlying data, and this advantage is able to effectively improve the historical data utilization. Overall, with the increase of PSP, the AE of FRGM-UPF decreases significantly. For instance, when the PSP equals to 100, the AEs of B06 and B07 are only 1 and 2 cycles, respectively.

For the prediction of P01 and S17 [see Fig. 7(c) and (d)], the results are relatively stable. There is no obvious discrimination between the predicted trajectory and the true value. The average values of AE for P01 and S17 are 6 and 4, respectively. However, for the results of S42 and S43 [see Fig. 7(e) and (f)], the prediction errors are relatively large. The maximum of AE is no more than 10. The discharge of dynamic current enables the discharge voltage to undulate more frequently, because the aging tests (see Fig. 2) contains complex discharge schedules. Likewise, the corresponding WPEE trajectories (see Fig. 4) display instable changing trend with fluctuations. Nevertheless,

due to the accumulated generating operation of FRGM, the randomness of the original WPEE data is weak and more deep characteristics are adopted to track the trends. Combining with the nonlinear filtering characteristics of UPF algorithm, the RUL prediction errors are controlled within ten cycles. Overall, prediction trajectories are highly consistent with the true values for various types of batteries under different conditions.

V. Conclusion

In this article, a synergy of the unique degradation indicator with an FRGM-UPF framework for RUL prediction has been explored. First of all, the WPEE captured the alteration of the discharge voltage to display the batteries' degradation. Second, a degradation model using FRGM for the WPEE was proposed to evaluate the degradation process as battery undertakes the charge/discharge cycles at various conditions. It has been proved that the model was efficient in fitting and prediction. Finally, the FRGM was employed to update the state transition equation in UPF and to establish an FRGM-UPF framework for RUL prediction. The experimental data from different types of batteries were adopted to verify the validity of method proposed by this study. The RUL prediction results indicate that the FRGM-UPF framework with WPEE has prominent performance with high accuracy and strong robustness for different batteries at complex aging conditions. The absolute errors are no more than ten cycles. The practicability and universality of the FRGM-UPF with WPEE for RUL prediction is precisely verified.

The developed technologies have practical implications to broaden the horizons of the battery management systems in the RUL prediction. Current work has proved that the WPEE of a complete discharge voltage curve can be used to characterize the degradation of batteries, but the voltage of batteries shows different trends at different discharge stages. Therefore, we will divide the discharge voltage curve of batteries into several intervals and extract the WPEE, respectively, from them to further explore the detailed degradation information in the following study. In addition, more information theory related knowledge will be applied to the processing of battery discharge voltage signal, aiming at providing a new way to find effective alternatives to the capacity for determination of the battery degradation state. But at the same time, the introduction of new algorithms will sometimes increase the computational burden. In future work, we will also take the optimization of algorithm complexity as an important research direction.

References

[1] W. He, N. Williard, M. Osterman, and M. Pecht, "Prognostics of lithium-ion batteries based on Dempster–Shafer theory and the Bayesian Monte Carlo method," *J. Power Sources*, vol. 196, pp. 10314–10321, 2011.

[2] Z. Yu, L. Xiao, H. Li, X. Zhu, and R. Huai, "Model parameter identification for lithium batteries using the coevolutionary particle swarm optimization method," *IEEE Trans. Ind. Electron.*, vol. 64, no. 7, pp. 5690–5700, Jul. 2017.

[3] G. Dong, Z. Chen, J. Wei, and Q. Ling, "Battery health prognosis using Brownian motion modeling and particle filtering," *IEEE Trans. Ind. Electron.*, vol. 65, no. 11, pp. 8646–8655, Nov. 2018.

[4] G. L. Plett, "Extended Kalman filtering for battery management systems of LiPB-based HEV battery packs," *J. Power Sources*, vol. 134, pp. 277–292, 2004.

[5] J. Zhang and J. Lee, "A review on prognostics and health monitoring of Li-ion battery," *J. Power Sources*, vol. 196, pp. 6007–6014, 2011.

[6] X. Hu, J. Jiang, D. Cao, and B. Egardt, "Battery health prognosis for electric vehicles using sample entropy and sparse Bayesian predictive modeling," *IEEE Trans. Ind. Electron.*, vol. 63, no. 4, pp. 2645–2656, Apr. 2016.

[7] Y. Zhou, M. Huang, Y. Chen, and Y. Tao, "A novel health indicator for on-line lithium-ion batteries remaining useful life prediction," *J. Power Sources*, vol. 321, pp. 1–10, 2016.

[8] Y. Zhang, R. Xiong, H. He, and M. G. Pecht, "Lithium-ion battery remaining useful life prediction with box–cox transformation and Monte Carlo simulation," *IEEE Trans. Ind. Electron.*, vol. 66, no. 2, pp. 1585–1597, Feb. 2019.

[9] K. Goebel, B. Saha, A. Saxena, J. Celaya, and J. Christophersen, "Prognostics in battery health management," *IEEE Instrum. Meas. Mag.,* vol. 11, no. 4, pp. 33–40, Aug. 2008.

[10] Q. Miao, L. Xie, H. Cui, W. Liang, and M. Pecht, "Remaining useful life prediction of lithium-ion battery with unscented particle filter technique," *Microelectron. Reliab.*, vol. 53, pp. 805–810, 2013.

[11] H. Zhang, Q. Miao, X. Zhang, and Z. Liu, "An improved unscented particle filter approach for lithium-ion battery remaining useful life prediction," *Microelectron. Reliab.*, vol. 81, pp. 288–298, 2018.

[12] C. Lyu, Q. Lai, T. Ge, H. Yu, L. Wang, and N. Ma, "A lead-acid battery's remaining useful life prediction by using electrochemical model in the particle filtering framework," *Energy*, vol. 120, pp. 975–984, 2017.

[13] A. Guha and A. Patra, "Online estimation of the electrochemical impedance spectrum and remaining useful life of lithium-ion batteries," *IEEE Trans. Instrum. Meas.*, vol. 67, no. 8, pp. 1836–1849, Aug. 2018.

[14] M. A. Patil *et al.*, "A novel multistage Support Vector Machine based approach for Li ion battery remaining useful life estimation," *Appl. Energy*, vol. 159, pp. 285–297, 2015.

[15] J. Wei, G. Dong, and Z. Chen, "Remaining useful life prediction and state of health diagnosis for lithium-ion batteries using particle filter and support vector regression," *IEEE Trans. Ind. Electron.*, vol. 65, no. 7, pp. 5634–5643, Jul. 2018.

[16] D. Liu, J. Zhou, D. Pan, Y. Peng, and X. Peng, "Lithium-ion battery remaining useful life estimation with an optimized relevance vector machine algorithm with incremental learning," *Measurement*, vol. 63, pp. 143–151, 2015.

[17] Y. Zhang, R. Xiong, H. He, and M. G. Pecht, "Long short-term memory recurrent neural network for remaining useful life prediction of lithium-ion batteries," *IEEE Trans. Veh. Technol.*, vol. 67, pp. 5695–5705, Jul. 2018.

[18] X. Li, L. Zhang, Z. Wang, and P. Dong, "Remaining useful life prediction for lithium-ion batteries based on a hybrid model combining the long short-term memory and Elman neural networks," *J. Energy Storage*, vol. 21, pp. 510–518, 2019.

[19] S. Tong, M. P. Klein, and J. W. Park, "On-line optimization of battery open circuit voltage for improved state-of-charge and state-of-health estimation," *J. Power Sources*, vol. 293, pp. 416–428, 2015.

[20] H. Lin, T. Liang, and S. Chen, "Estimation of battery state of health using probabilistic neural network," *IEEE Trans. Ind. Inform.*, vol. 9, no. 2, pp. 679–685, May 2013.

[21] D. Liu, J. Zhou, H. Liao, Y. Peng, and X. Peng, "A health indicator extraction and optimization framework for lithium-ion battery degradation modeling and prognostics," *IEEE Trans. Cybern.*, vol. 45, no. 1, pp. 915–928, Jun. 2015.

[22] X. Hu, S. E. Li, Z. Jia, and B. Egardt, "Enhanced sample entropy-based health management of Li-ion battery for electrified vehicles," *Energy*, vol. 64, pp. 953–960, 2014.

[23] B. Saha and K. Goebel, "Battery Data Set," NASA Ames Prognostics Data Repository, NASA Ames Research Center, Moffett Field, CA, USA, 2007. [Online]. Available: http://ti.arc.nasa.gov/tech/dash/groups/pcoe/prognostic-data-repository

[24] W. Chen, B. Xie, Z. Long, L. Cui, and X. Chen, "Stage identification in air-gap discharge of oil-impregnated paper insulation based on wavelet packet energy entropy," in *Proc. Chin. Soc. Elect. Eng.*, vol. 02, pp. 563–569, 2016.

[25] Z. Liu, Q. Hu, Y. Cui, and Q. Zhang, "A new detection approach of transient disturbances combining wavelet packet and Tsallis entropy," *Neurocomputing*, vol. 142, pp. 393–407, 2014.

[26] Y. Zhang, W. Wei, and W. Lin, "Motor mechanical fault diagnosis based on wavelet packet, Shannon entropy, SVM and GA," *Elect. Power Automat. Equip.*, vol. 1, pp. 87–91, 2010.

[27] J. Ma, J. Wu, and X. Wang, "Fault diagnosis method based on wavelet packet-energy entropy and fuzzy kernel extreme learning machine," *Adv. Mech. Eng.*, vol. 10, pp. 1–14, 2018.
[28] Y. Zhang, R. Xiong, H. He, and M. G. Pecht, "Lithium-ion battery remaining useful life prediction with box–cox transformation and Monte Carlo simulation," *IEEE Trans. Ind. Electron.*, vol. 66, no. 2, pp. 1585–1597, Feb. 2019.
[29] H. Pan, Z. Lü, W. Lin, J. Li, and L. Chen, "State of charge estimation of lithium-ion batteries using a grey extended Kalman filter and a novel open-circuit voltage model," *Energy*, vol. 138, pp. 764–775, 2017.
[30] L. Chen, W. Lin, J. Li, B. Tian, and H. Pan, "Prediction of lithium-ion battery capacity with metabolic grey model," *Energy*, vol. 106, pp. 662–672, 2016.
[31] J. L. Deng, "Control problems of grey systems," *Syst. Control Lett.*, vol. 1, pp. 288–294, 1982.
[32] Y. Chen, L. Li, H. Peng, J. Xiao, and Q. Wu, "Dynamic multi-swarm differential learning particle swarm optimizer," *Swarm Evol. Comput.*, vol. 39, pp. 209–221, 2018.
[33] L. Zhang, Z. Mu, and C. Sun, "Remaining useful life prediction for lithium-ion batteries based on exponential model and particle filter," *IEEE Access*, vol. 6, pp. 17729–17740, 2018.

Lin Chen received the M.S. degree in computer applied technology from Guangxi University, Nanning, China, in 2004 and the Ph.D. degree in biomedical engineering from the Huazhong University of Science and Technology, Wuhan, China, in 2008.

Since 2011, she was a Professor with the College of Mechanical Engineering, Guangxi University, Nanning, China. She has hosted and participated in as many as ten national or regional fund projects. She has authored and coauthored more than 50 technical papers and holds more than 20 patents. Her research interests include automation and control, robotics, digital signal detection and processing, ac servo drives, battery management technology, and other related research work.

Jing Chen is currently working toward the M.S. degree in mechanical engineering with Guangxi University, Nanning, China.

Her research interests include the battery management system in electric vehicles.

Huimin Wang received the Bachelor's degree from the School of Mechatronics Engineering, Harbin Institute of Technology, Harbin, China, in 2016. He is currently working toward the M.S. degree in mechatronic engineering with Guangxi University, Nanning, China.

His research interests include the battery management system in electric vehicles.

Yijue Wang received the M.Sc. degrees in statistics in 2017 from the University of Connecticut, Storrs, CT, USA, where he is currently working toward the Ph.D. degree in computer science.

Since 2015, he has worked on risk prediction problem with statistical analysis and machine learning algorithm with USA Insurance Company and Pharmacy Company. He has worked on different projects about closest pair algorithm and membership privacy with deep learning model as a research assistant. His research interests include membership attack protection in machine learning model, closest pair algorithm, and battery management.

Jingjing An is currently working toward the M.S. degree in power machinery and engineering with Guangxi University, Nanning, China.

His research interests include battery management system in electric vehicles.

Rong Yang received the Ph.D. degree in power machinery and engineering from Tongji University, Shanghai, China, in 2015.

Since 2016, she has been a Lecturer of vehicle engineering with Guangxi University, Nanning, China. Her research interests include control strategies for hybrid electric vehicles, automatic driving control technology based on image recognition, testing and analysis technology for diesel engine combustion characteristics in transient conditions.

Haihong Pan received the Ph.D. degree in mechanical engineering from the Huazhong University of Science and Technology, Wuhan, in 2007.

Since 2008, he has been a Professor with the College of Mechanical Engineering, Guangxi University, Nanning, China. He has hosted and participated in as many as 16 national or regional fund projects. He has authored and coauthored more than 60 technical papers and been granted with more than 50 patents. His research interests include electromechanical control theory and method of complex electromechanical systems, all digital networked ac servo drive motor control theory and technology, and other related research work.